Research paper

Out-of-plane mechanical behaviors of a side hierarchical honeycomb

Yong Zhang[a,*], Tengteng Chen[a], Xiang Xu[b], Zhongwei Hu[a]

[a] *College of Mechanical Engineering and Automation, Huaqiao University, Xiamen, China*
[b] *School of Automotive Studies, Tongji University, Shanghai, China*

ABSTRACT

Hierarchical honeycombs have been extensively used as protective devices due to their superior mechanical performance. In this paper, a novel side hierarchical triangular honeycomb (SHTH) constructed by sequentially arranging a certain number of similar subtriangles on the geometrical side of an ordinary triangular honeycomb (OTH) is proposed to enhance structural mechanical performance. Experimental specimens and finite element models of SHTHs are developed to explore their mechanical behaviors under out-of-plane compression, and the numerical models are validated based on the results of crushing tests of SHTHs. Numerical comparisons of the SHTH, OTH and double-triangular honeycomb (DTH) are performed and illustrate that the SHTH has a higher collision force level and better energy absorption than the OTH and DTH due to more stable collapse deformation. Moreover, a parametric investigation of the SHTH is performed to explore the influences of the relative density, hierarchical factor and layout of the honeycomb on crashworthiness. The results show that the crashworthiness of the SHTH is improved with increasing relative density and number of layouts. Furthermore, the stable energy absorption and load bearing efficiency of the SHTH are observed when the hierarchical factor is close to 10. A theoretical model of the SHTH is also derived and validated based on simplified super folding element theory (SSFE) and numerical analysis. The findings of this study provide a new method for designing an energy absorber with excellent protective performance.

1. Introduction

Honeycomb structures, as typical porous lightweight materials, have been widely used in vehicle (Wang et al., 2016), aerospace (Meng et al., 2009) and ship design (Crupi et al., 2013) due to their potential multifunctional applications and specific in-plane and out-of-plane mechanical properties (Ashab et al., 2015; Hohe and Becker, 2003; Lee et al., 2002; Sezgin et al., 2010; Zhi, 2016). A large number of studies of the energy absorption (EA) (Baroutaji et al., 2017; Yang et al., 2018a; Yin et al., 2018), bending (Abo Sabah et al., 2017), blasting (Liu et al., 2018; Sun et al., 2019), and fatigue (Belouettar et al., 2009) of honeycomb structures have been performed and have found that honeycomb structures have excellent mechanical properties. At present, researchers are beginning to explore some new methods for designing honeycomb structures to meet higher requirements in protective performance.

Bionic design is an effective means of improving the mechanical performance of honeycomb structures. For example, Hao and Du (2018) and Xiang and Du (2017) were inspired by the beetle to propose new bioinspired honeycomb thin-walled structures by embedding circular columns in different places (as shown in Fig. 1(a)). They found that

bioinspired honeycombs were obviously better than traditional hexagonal honeycombs in terms of mechanical properties. Yang et al. (2018b) explored a novel bioinspired honeycomb (Fig. 1(b)) composed of horseshoe microstructures and found that the addition of horseshoe cells to a conventional honeycomb improved specific energy absorption. Moreover, the hierarchical organization of biomaterials also attracts significant interest from researchers interested in designing novel hierarchical honeycombs with better mechanical performance (An et al., 2014; Chen et al., 2014; Korsunsky, 2014; Murthy et al., 1993; Sun et al., 2016a; Sun and Pugno, 2013; Zhang et al., 2018d). For example, researchers first investigated the basic physical properties of hierarchical honeycomb materials. Taylor et al. (2011, 2012) found that a hierarchical honeycomb with an in-plane thickness gradient can improve the elastic modulus. Sun and Pugno (2013) revealed that the in-plane stiffness of a hierarchical honeycomb with a negative Poisson's ratio was nearly 100 times greater than that of a traditional honeycomb. Ajdari et al. (2012) found that the hardness values of first- and second-order vertex hierarchical honeycombs were 2.0 and 3.5 times higher, respectively, than that of a traditional honeycomb with the same mass.

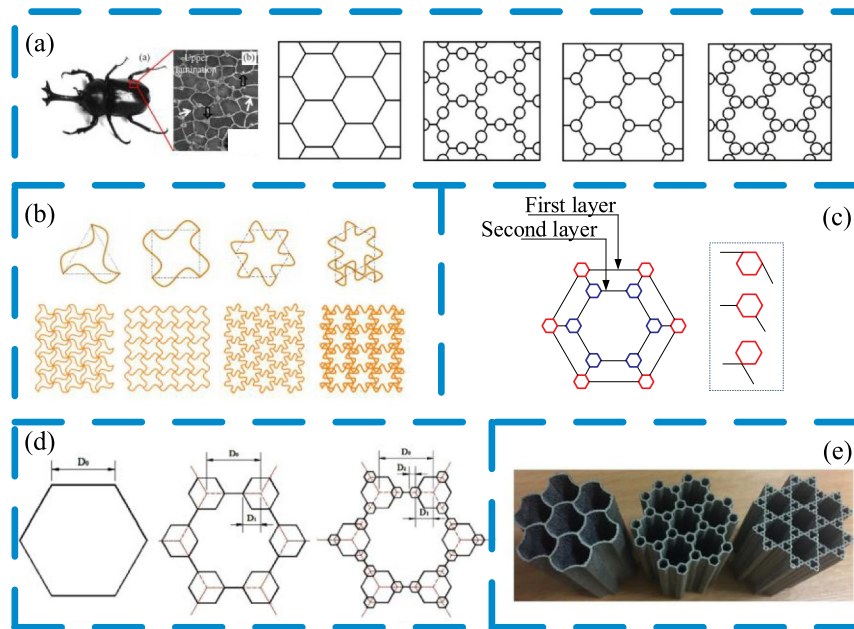The EA characteristics of hierarchical honeycombs have also been

---

Fig 1. Design of bionic honeycombs and hierarchical honeycombs: (a) (Hao and Du, 2018); (b) (Xiang and Du, 2017); (c) (Zhang et al., 2018d); (d) (Sun et al., 2016b; Zhang et al., 2016); (e) (Zhang et al., 2018c).

explored in recent years (Fan et al., 2018; Fang et al., 2018; Xu et al., 2019). For example, Zhang et al. (2018d) explored the effect of fractal configurations of double hexagonal honeycomb structures on crashworthiness under an out-of-plane impact. They found that the inner subhexagons in the first layer and central subhexagons in the second layer provided the optimal hierarchical configuration (see **Fig. 1(c)**). Sun et al. (2016b) investigated the influence of the structural parameter θ of a vertex hierarchical honeycomb on crashworthiness (**Fig. 1(d)**). The results showed that hierarchical honeycombs with angles θ from 30° to 50° had better energy absorption than other angles θ in an out-of-plane dynamic crash. Moreover, Zhang et al. (2016) found that the specific energy absorption of a hierarchical honeycomb increased with wall thickness, and a dimension of 9 × 9 had better mechanical properties among hierarchical honeycombs subjected to an out-of-plane impact. Zhang et al. (2018c) carried out a dynamic out-of-plane compressive analysis of a hierarchical hexagon honeycomb obtained via selective laser sintering (SLS) technology and found that the EA capacity of the hierarchical hexagon honeycomb was significantly greater than that of a single honeycomb (**Fig. 1(e)**). To summarize, the abovementioned studies have shown that hierarchical design is an effective means of improving the mechanical properties of traditional honeycombs.

Previous studies focused mainly on the mechanical behaviors of vertex hierarchical hexagonal honeycombs. However, research on the crashworthiness of honeycomb structures with different geometrical topologies and hierarchical designs is scarce. Based on the above observations, this paper proposes a new side hierarchical triangular honeycomb (SHTH) and investigates its out-of-plane crushing performance via experimental testing and theoretical prediction. Section 2 first gives a description of the side hierarchical method, and a new hierarchical honeycomb is presented. Section 3 performs an experiment and numerical simulation of the honeycomb. Crashworthiness behaviors of a hierarchical triangular honeycomb, ordinary triangular honeycomb (OTH), and double-triangular honeycomb (DTH) are investigated and compared in Section 4. A parametric investigation of this novel hierarchical honeycomb is performed in Section 5. Finally, a theoretical model for the SHTH under an out-of-plane impact is developed in Section 6.

2. Design of the SHTH

2.1. The side hierarchical design

The side hierarchical design can be obtained by arranging a certain number (N) of self-similar subcells on the geometrical side of a primary cell, N is also called a hierarchical factor. Taking a triangular primary cell as an example, the side of this triangle can be replaced by using 2 to N subtriangles to form different hierarchical designs. The design process is illustrated in **Fig. 2**.

2.2. The geometrical characteristics of the side hierarchical honeycombs

According to the side hierarchical design shown in **Fig. 2**, an SHTH based on the ordinary triangular honeycomb (OTH) is proposed in **Table 1**. The side length of a subtriangle is l, and the triangle marked by the red line can be regarded as the primary structure of the subtriangles, in which L is equal to $N \times l$. L is the side length of the primary triangle and OTH; N is the hierarchical factor of the SHTH, and the wall thickness of the honeycomb is t.

Table 1 presents the geometric model of the SHTH and OTH arranged in a 4 × 3 layout (there are four and three original triangles arranged in the horizontal and vertical directions, respectively) to investigate the crashworthiness under an out-of-plane impact. Moreover, a double-triangular honeycomb (DTH) is also established to investigate the difference of crashworthiness, and the DTH has the same side length L_1 of the inner triangle as the SHTH. L_1 is determined by the hierarchical factor N and $L_1 = L*(N-3)/N$ ($N \geq 4$); for example, L_1 is
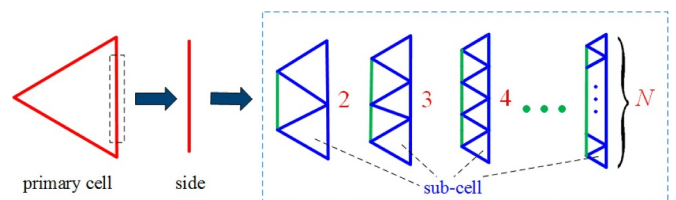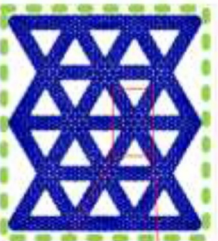

Fig 2. The side hierarchical design of the triangular primary cell.

Table 1
Geometric characteristics of the different honeycombs.

18.75 mm if N and L are 8 and 30 mm, respectively. The out-of-plane height h of the honeycomb is 50 mm. In addition, Table 1 provides a list of acronyms with their definitions for the SHTH, OTH and DTH.
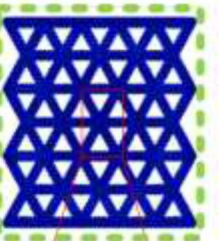
3. Experimental specimens and numerical modeling

3.1. Experimental specimens and preparation

A honeycomb structure SHTH$_2$ (N = 2) with a layout of 2 × 2 and a primary triangle substructure PC-SHTH$_5$ (N = 5) were prepared as experimental specimens. The preparation process is shown in Fig. 3(a). The 6060-T4 aluminum alloy block was machined by wire-cut electrical discharge machining (WEDM) to obtain honeycomb specimens; WEDM is a thermal machining process involving electrical spark discharge and continuously moving the electrode wire to cut the aluminum alloy block. The obtained specimens are shown in Fig. 3(b). The height h, wall thickness t and side length L of the primary triangle substructure are 50 mm, 0.5 mm and 30 mm, respectively.

A crushing test is a common method to investigate the EA capacity of thin-walled structures (Chen et al., 2019; Fang et al., 2015a, 2015b; Zhang et al., 2018e). Therefore, a quasi-static crushing test is carried out using a universal material testing machine (UMTM). The maximum force of the upper impact device is 300 kN, and the speed is 5 mm/min, as shown in Fig. 4. One end of the specimen is fixed on the supporting platform, and the other end bears the compression force until the crushing displacement is 25 mm. Video is used to record the crushing process, and the data collection system is used to gather the force and displacement data values during the crushing process.
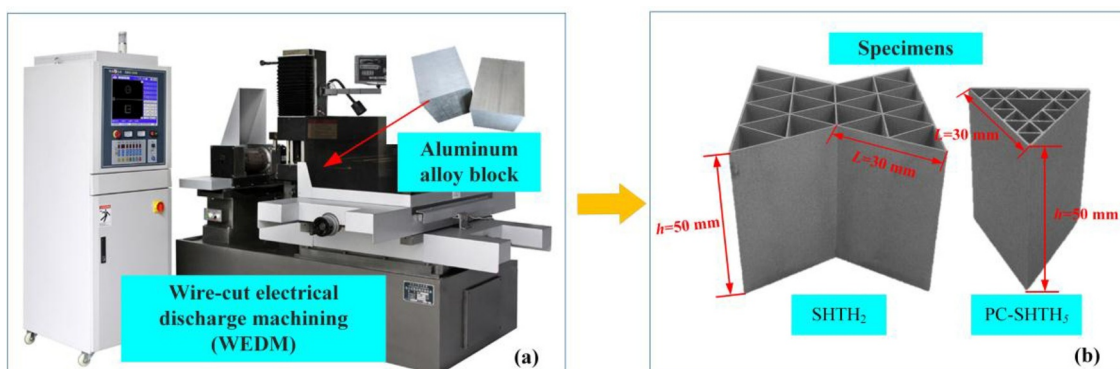

Fig 3. Experimental preparations: (a) wire-cut electrical discharge machine; (b) specimens: SHTH$_2$ and PC-SHTH$_5$.
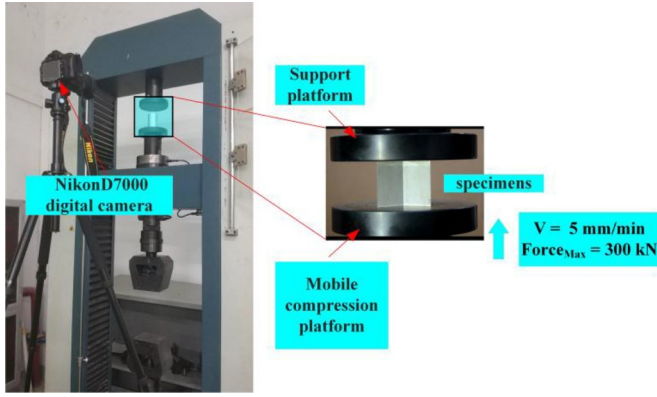
Fig 4. Universal material testing machine and boundary condition.

3.2. Numerical modeling

The dynamic impacting models of three honeycomb structures (OTH, DTH and SHTH) were established in **Fig. 5** according to the geometric model described in **Table 1** using the nonlinear explicit finite element (FE) software package LS-DYNA 971. LS-DYNA is a nonlinear finite element analysis software owned and developed by Livermore Software Technology Corporation (LSTC). The size of the mesh of the FE models for all structures was set to 1 mm × 1 mm to comprehensively consider the calculation cost and the accuracy of the model. The impact models of honeycomb structures were developed and shown in **Fig. 5(d)**, where a rigid impactor of 200 kg impacted axially the honeycomb supported on a rigid wall at a velocity of 10 m/s. The impactor and rigid wall were regarded as rigid bodies and meshed with 8-node solid elements. The material models MAT_123 and MAT_20 in LS-DYNA were adopted to model the honeycomb and the impactor, respectively, in which Mat_123 is a piecewise linear plasticity material. The material model was defined as having nonlinear isotropic work hardening in the plastic region (Hallquist, 2003). The von Mises yield criterion was used as

$$\phi = J_2 - \frac{\sigma_y^2}{3} \tag{1}$$

where the second stress invariant J_2 is defined in terms of the deviatoric stress components as
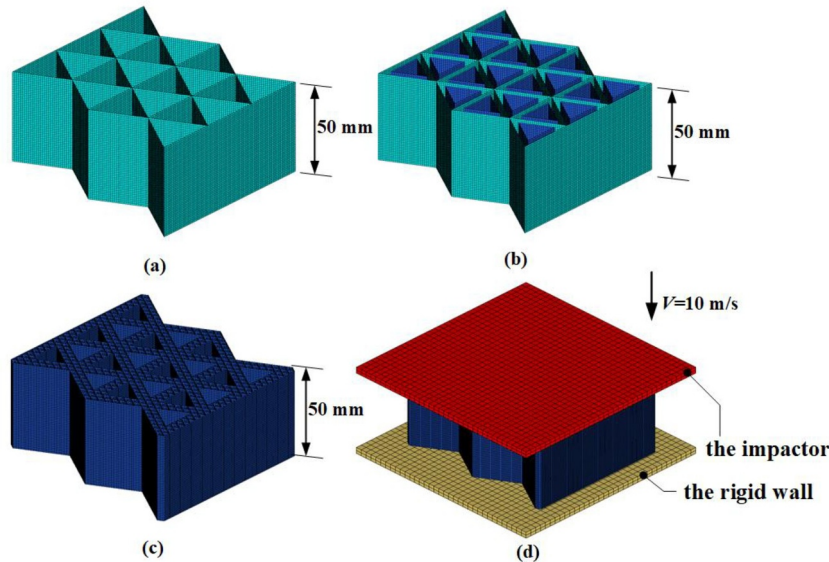
Table 2
Mechanical parameters of AA6060-T4.

Material parameters	Symbol	Value
Young's modulus	E	68.2 GPa
Density	ρ	$2.7 \times 10^3 \, \text{kg/m}^3$
Poisson's ratio	μ	0.3
Initial yield stress	σ_y	80 MPa
Ultimate stress	σ_u	173 MPa
Power law exponent	n	0.23

$$J_2 = \frac{1}{2} s_{ij} s_{ij} \tag{2}$$

and the yield stress σ_y can be defined as

$$\sigma_y = \sigma_o + f_h(\varepsilon_{eff}^p) \tag{3}$$

where σ_o is the initial yield stress and $f_h(\varepsilon_{eff}^p)$ is the hardening function.

Automatic single surface and automatic node to surface contact were set to simulate the self-contact condition of the honeycomb and the contact relationship between the impactor and honeycomb, respectively. The coefficients of dynamic friction and static friction in all models were set to 0.2 and 0.3, respectively, to account for the contact friction problem in the actual situation (Wang et al., 2018).

The material of the honeycomb structure is 6060-T4 aluminum alloy, and the basic mechanical properties are reported in **Table 2**. The engineering stress-strain curve of 6060-T4 was obtained in (Zhang et al., 2018a). In addition, this paper ignored the influence of strain rate because the strain rate sensitivity of aluminum alloys was weak (Zhang et al., 2014).

3.3. Experimental results and validation of the numerical model

3.3.1. Evaluation indicators

Several crashworthiness indicators are introduced to evaluate the mechanical properties of the honeycomb structures.

1) Specific energy absorption (SEA): the energy absorption of honeycomb materials per unit mass (Zhang et al., 2018e).

$$\text{SEA} = \frac{\text{EA}}{m} \tag{4}$$

Fig 5. FE models: (a) OTH; (b) DTH; (c) SHTH; (d) dynamic impact model.

where EA is the total energy absorption of the structure during the crushing process, computed as $EA = \int_0^S F(x) \, dx$; where $F(x)$ is the instantaneous collision force and S is the collapse displacement; m is the total mass of the honeycomb.

1) Peak crushing force (PCF): the maximum value of the crash force of the honeycombs in the external load.
2) Mean crushing force (MCF): the average value of the collision force of the honeycomb during the crushing process,

$$MCF = (\int_0^S F(x) \, dx)/S \tag{5}$$

Crushing load efficiency (CLE): the load bearing stability of the structure in the crushing process, which is expressed by the formula (Fang et al., 2017):

$$CLE = \frac{MCF}{PCF} \times 100\% \tag{6}$$

A CLE close to 1 is the most desirable because it indicates a reasonably low PCF with a high EA or a high MCF.

3.3.2. Experimental responses of the SHTH

Fig. 6 shows the force-displacement curves of the two specimens. First, the collision forces of SHTH$_2$ and PC-SHTH$_5$ exhibit a sharp upward trend in the initial impacting stage because the honeycomb has an elastic phase. Next, the honeycomb structures begin to yield when the impact force reaches a peak force PCF (point A or a). Then, the honeycomb structures begin to collapse, and the collision force maintains a stable level. Moreover, the collapse force rises because the structure has been compacted when the displacement exceeds 23 mm for PC-SHTH$_5$ (point g).

Fig. 7(a) and (b) show that SHTH$_2$ and PC-SHTH$_5$ are crushed layer-by-layer during the crushing process. The collapse shape is believed to be an efficient EA mode (Wu et al., 2016). For SHTH$_2$, deformation starts from the lower middle part of the test specimen and then undergoes a stable fold. In terms of PC-SHTH$_5$, the progressive collapse process is triggered at the bottom end, followed by regular folds stacking onto the first fold.

The basic component of specimen SHTH$_2$ is selected and shown in the red box in Fig. 8 to simply compare the deformation shapes when N is 2 and 5. Obviously, three folded waves are formed in the basic component of specimen SHTH$_2$ with $N = 2$ as the quasi-static compressive distance is kept fixed to 25 mm. However, the number of folded waves increases to five when $N = 5$, and compared with the case of $N = 2$, the folding wavelength decreases. This result indicates that hierarchical factor N has an important effect on the mechanical behavior of a side hierarchical honeycomb.
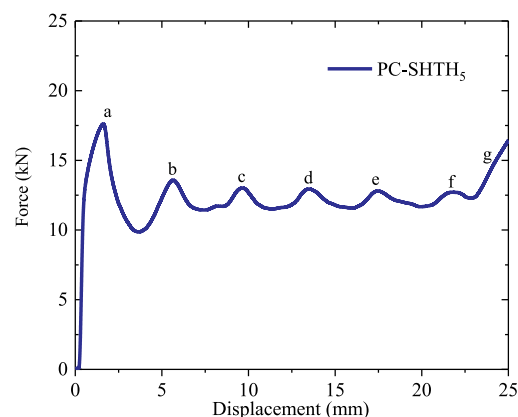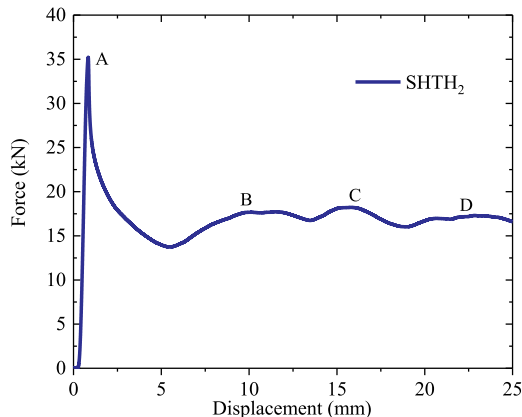
The force-displacement curves shown in Fig. 6 can be used to calculate crashworthiness indicators of the two specimens, which are listed in Table 3.

3.3.3. Verification of FE models

Numerical models of quasi-static compression are established according to the geometric dimensions of SHTH$_2$ and PC-SHTH$_5$ specimens. The compression speed is set as 5 mm/min, in line with the experiment. Fig. 9 presents the deformation comparisons of the numerical and experimental results. Obviously, both the front view and the top view (Fig. 9(a) and (b)) of the experimental testing and the crushing simulation of SHTH$_2$ and PC-SHTH$_5$ show a very similar collapse mode.

Fig. 10 further shows the comparisons of the force-displacement curves for the simulation and the experimental data. Fluctuations of the force-displacement curves of the simulations agree well with the experimental results. Furthermore, the results of numerical predictions and errors are reported in Table 4. It can be observed that the maximum error of the simulation value and the experimental value is 7.43%. Consequently, the FE models developed in this paper are considered reliable for investigating the EA behaviors of the SHTH.

4. Crashworthiness comparison of three honeycombs

The OTH and DTH are compared with the SHTH to reveal the difference in mechanical properties under an out-of-plane impact. The parameters L and h are 30 mm and 50 mm, respectively, and t needs to be changed to keep the same mass, 34.91 g. The relevant boundary conditions of the numerical models are consistent with those described in Section 3.2.

Fig. 11 presents force-displacement curves and SEAs of the three honeycomb structures. Apparently, the OTH, DTH, and SHTH have a stable plateau stage during the out-of-plane compression. The initial peak force of the SHTH is almost the same as those of the OTH and DTH. However, the SEA of the SHTH is at the highest level, and its growth rate maintains a high stable trend with the folding process, as can be observed from Fig. 11(b). This result indicates that the SHTH has the best crashworthiness characteristics among three honeycomb structures of the same mass. The reasons can be revealed by deformation modes shown in Fig. 12 of the three honeycomb structures at different crushing displacements. The OTH and DTH structures have similar deformation modes, and the folding wave is transmitted from top to bottom as the compression progresses, but the folds of the OTH and DTH are irregular under an out-of-plane impact. However, the SHTH forms a global folding wave in the impact process, and the compressive wave behaves regularly from beginning to end, which indicates that the SHTH has a more stable mechanical response under resisting external loads (see Fig. 12(b)).

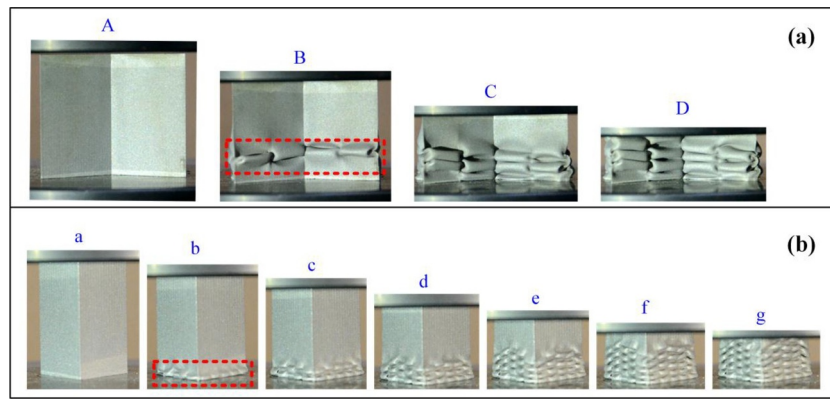Furthermore, the OTH has a larger SEA and a higher crushing force

Fig 6. Force-displacement curves obtained via experimental tests: (a) SHTH$_2$; (b) PC-SHTH$_5$.

Fig 7. Deformation shapes of experimental specimens at different axial displacements: (a) SHTH$_2$; (b) PC-SHTH$_5$.
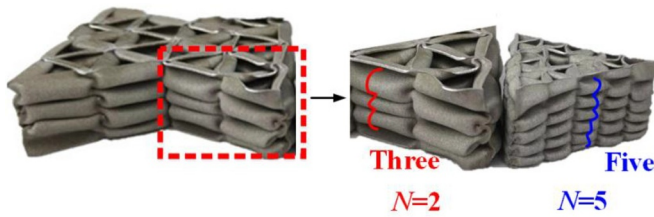

Fig 8. Deformation comparison of the basic component with different hierarchical factor N.

Table 3
Experimental results of SHTH$_2$ and PC-SHTH$_5$ under quasistatic crushing.

Structure	SEA (kJ/kg)	PCF (kN)	MCF (kN)	CLE	Mass (g)
SHTH$_2$	11.57	35.20	16.87	0.48	36.3
PC-SHTH$_5$	23.91	17.60	12.24	0.70	10.5

level than the DTH of the same mass; therefore, the energy absorption capacity of the honeycomb structure cannot be improved by simply adding a subcell such as in the DTH, but the side hierarchical design is a more effective means of improving the crashworthiness of honeycomb structures.

Table 5 further presents the values of crashworthiness indicators for the three honeycomb structures. On the one hand, the SEA and CLE of the SHTH are improved by 79.3% and 90% compared with the OTH, respectively. On the other hand, the crashworthiness performance of the DTH is inferior to the OTH because the SEA and CLE of the DTH

decrease by 35% and 34% compared with the OTH. Meanwhile, the PCF of the SHTH presents a slight downward trend compared with those of the OTH and DTH. Therefore, the results demonstrate that the side hierarchical design of a honeycomb structure has apparent crashworthiness advantages over a nonhierarchical design (ordinary structure).

5. Parametric analysis of the SHTH

After the comparative analysis in Section 4, we found that compared with the other honeycomb structures, the SHTH has excellent crashworthiness, and to comprehensively exhibit the mechanical performance of the SHTH, a parametric study is carried out in this section. The boundary conditions of the numerical analysis are the same as those described in Section 3.2.

5.1. Influence of the relative density

The relative density is an important parameter affecting the mechanical behavior of porous materials (such as honeycombs) (Balawi and Abot, 2008; Fang et al., 2018; Zhang et al., 2018b; Zhu, 2010). The relative density ρ_d of a honeycomb is calculated as the ratio of the filled material volume to the total occupied volume of unit cells. That is,

$$\rho_d = \frac{\rho^*}{\rho_s} = \frac{V_s}{V} \tag{7}$$

where ρ^* is the apparent density of the honeycomb structure; V is the volume occupied by the basic unit of the honeycomb (as shown in the
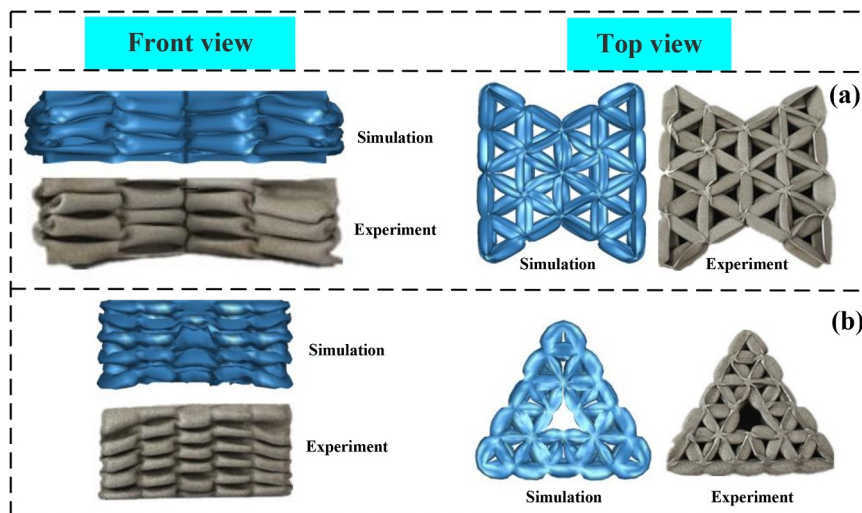

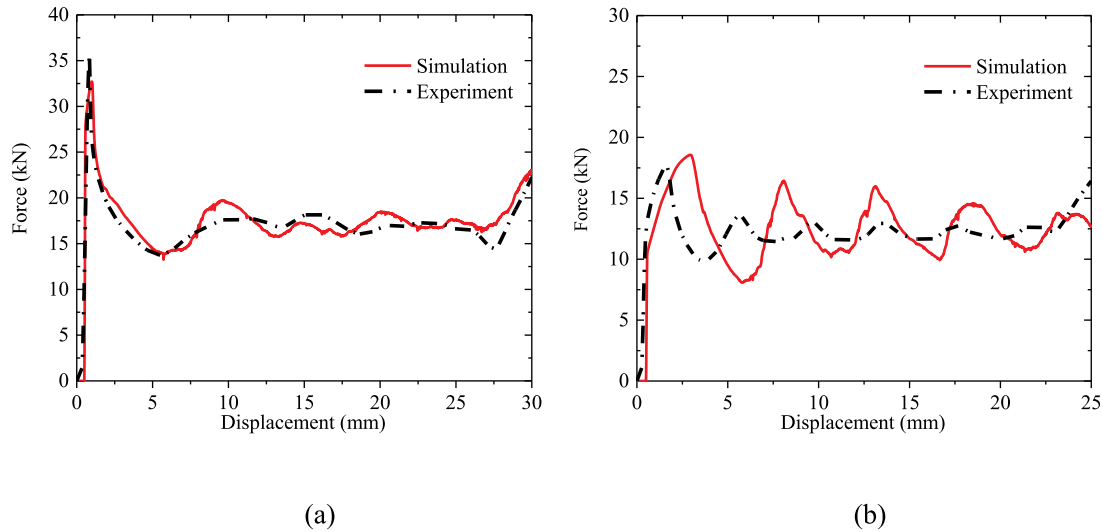**Fig. 9.** Deformation comparison of experiment and simulation; (a) SHTH$_2$; (b) PC-SHTH$_5$.

(a)   (b)

Fig 10. Comparison of experimental and simulated force-displacement curves: (a) $SHTH_2$; (b) PC-$SHTH_5$.

Table 4
Numerical results (FEA) and error of $SHTH_2$ and PC-$SHTH_5$.

Structure	SEA (kJ/kg) FEA	PCF (kN) Error (%)	FEA	MCF (kN) Error (%)	FEA	Error (%)
$SHTH_2$	10.71	−7.43	32.60	−7.39	17.97	6.52
PC-$SHTH_5$	22.82	−4.56	18.56	5.45	12.41	1.39

blue hexagonal basic cell of **Fig. 13**); ρ_s is the density of the honeycomb base material, and Vs is the actual volume of the base material.

By analyzing the configuration characteristics of the SHTH, V and Vs for the SHTH can be expressed as follows:

$$V = \frac{L}{2}\tan(\frac{\pi}{6})\cdot\frac{L}{2}\cdot 6\cdot h = \frac{3}{2}L^2 h \tan(\frac{\pi}{6}) = \frac{3}{2}N^2 l^2 h \tan(\frac{\pi}{6}) \tag{8}$$

$$V_s = (21\cdot N - 36)\cdot l\cdot h\cdot t \tag{9}$$

Thus, the relative density ρ_d of the SHTH is calculated by substituting Eqs. (8) and (9) into Eq. (7):

$$\rho_d = \frac{\rho^*}{\rho_s} = \frac{V_s}{V} = \frac{(21N\cdot l - 36l)\cdot h\cdot t}{\frac{3}{2}N^2 l^2 h \tan(\frac{\pi}{6})} = \frac{2\sqrt{3}(7N - 12)}{N^2}\cdot\frac{t}{l} \tag{10}$$

The relative density of the side hierarchical honeycomb is mainly related to the hierarchical factor N and the thickness t (when N is fixed, l is equal to $30/N$).

The EA values of the SHTHs with the 4×3 layouts and $N = 8$ under the different relative densities are shown in **Fig. 14(a)**. Apparently, the EAs of the SHTHs improve significantly as ρ_d increases. **Fig. 14(b)** plots the force and displacement curves of SHTHs under four relative densities. Both the initial peak force and the plateau force follow an upward trend with the compressive process because an increase of relative density causes an increase in the stiffness of the honeycomb structure. Specifically, the collision force exhibits an upward with the compressive process because the honeycomb structure gradually enters the densification stage, as shown in **Fig. 14(b)**. Furthermore, an increase in relative density clearly leads to the early arrival of the densification stage of the honeycomb structures.

Table 6. summarizes the values of the crashworthiness indicators of the SHTH. The increments of SEA and CLE are approximately 53% and 45%, respectively, when the relative density increases from 0.025 to 0.064, which means that it is helpful to increase the relative density of the honeycomb to improve its crashworthiness.

Table 7. exhibits the deformation shapes and plastic strain shapes of SHTHs of different relative densities. SHTHs produce stably folded waves and a high strain region under a crushing load. Moreover, the folding lobe and the high strain region are mainly concentrated in the top end of the structure when the relative density is 0.025. As the relative density increases, the fold lobe and the high strain region of the top end gradually reduce, but the bottom end exhibits the opposite behavior. This result indicates that the deformation mode of the side
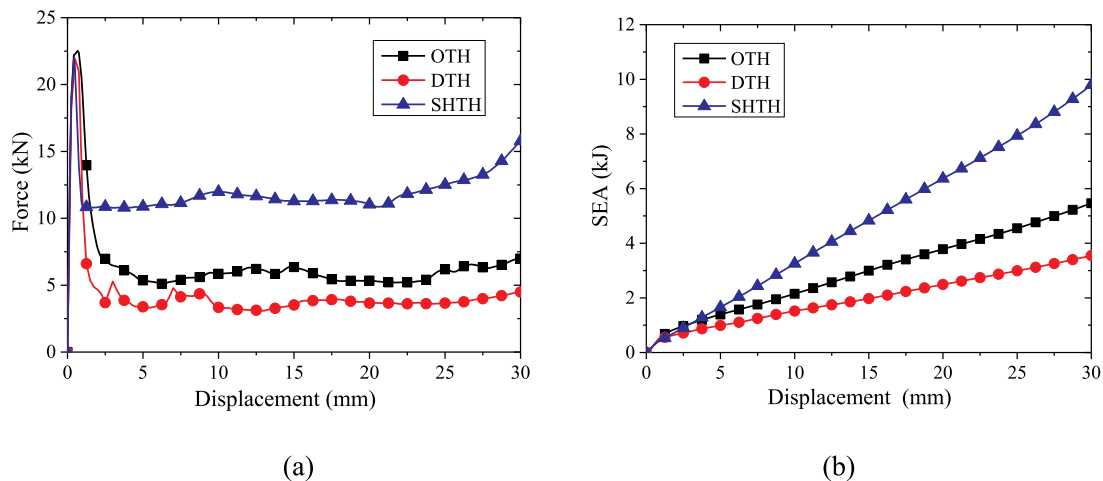

(a)   (b)

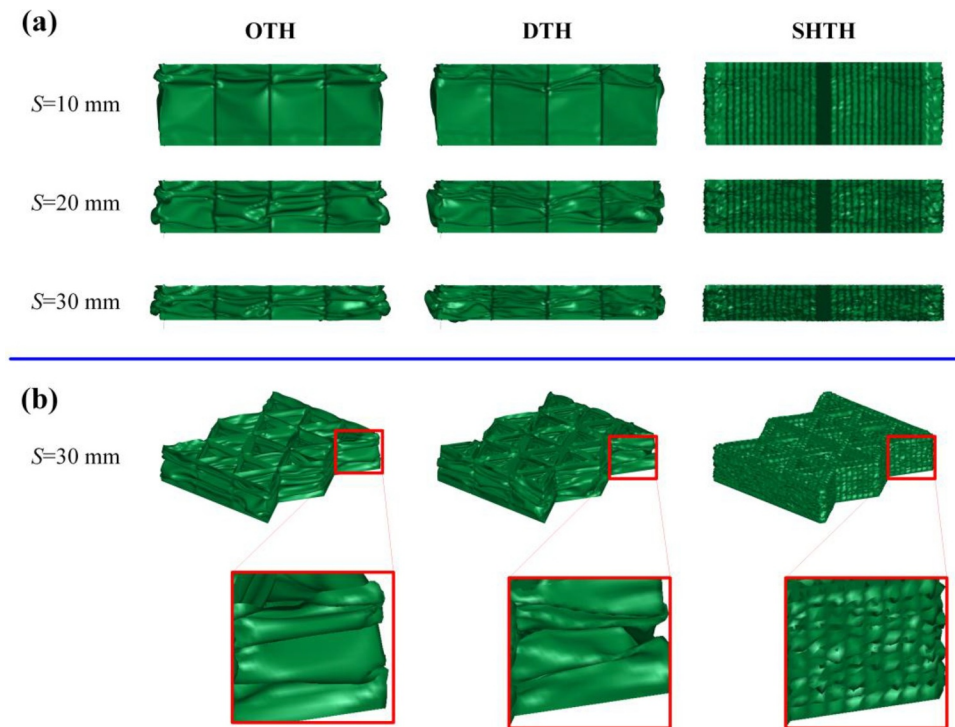**Fig 11.** Numerical simulation results: (a) force-displacement curves; (b) specific energy absorption (SEA).

Fig 12. Simulation results: (a) deformation shapes of three honeycombs at different crushing displacements; (b) local enlarged figures of deformation shape at crushing distance of 30 mm.

Table 5
Crashworthiness indicators of the three honeycomb structures.

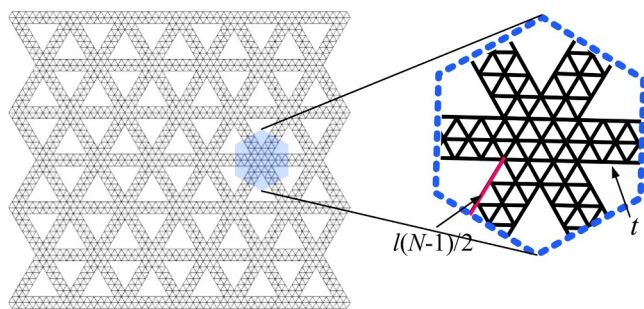| Honeycomb structures	EA (J)	SEA (kJ/kg)	MCF (kN)	PCF (kN)	CLE (%)
OTH	190.77	5.46	6.36	22.37	28.43
DTH	123.92	3.55	4.13	21.93	18.83
SHTH	341.89	9.79	11.39	21.09	54.01

Fig 13. The basic unit of the side hierarchical honeycomb.

hierarchical honeycomb gradually transitions from deformation at one end to both ends synchronously with the increase in relative density. Both ends of folding deformation are favorable for absorbing kinetic energy for the SHTH. Hence, it is concluded that with increasing relative density, the collapse of the honeycomb structure changes from one end to both ends, and this deformation is conducive to EA.

5.2. Effect of the hierarchical factor (N)

N is the number of subtriangles arranged on the side of the primary triangles of the SHTH, which is a key parameter for determining the geometric shape of the SHTH. Therefore, this section investigates the crashworthiness influence of the hierarchical factor from 4 to 12 of SHTH under the out-of-plane impact. The relative density ρ_d is 0.025.

Fig. 15(a) summarizes the force-displacement curves of the SHTH with different hierarchical factors. It is obvious that the collapse force increases first and then becomes stable when N changes from 4 to 12. The variation trends of the SEA, PCF, and CLE of SHTHs with different N are shown in Fig. 15(b) to (d). Obviously, the EA and load bearing efficiency of the SHTH increase gradually with increasing in N. The maximum SEA and CLE are observed when N is close to 10, and the maximum SEA and CLE increments of the SHTH are 79.63% and 80%, respectively. However, the increase in SEA and CLE is obviously reduced when N is over 10. The increments of SEA and CLE are only 1.62% and 0.96%, respectively, when N changes from 10 to 12, which shows that the SEA and CLE of the SHTH approach the maximum and become stable when N is more than 10. Moreover, the PCF exhibits a trend of horizontal stability under different N because the relative density ρ_d is constant for the SHTH.

(b) specific energy absorption, SEA; (c) peak crushing force, PCF; (d) crushing load efficiency, CLE.

Fig. 16 shows the deformation shapes of the SHTHs when the hierarchical factor N increases from 4 to 12. Apparently, the SHTHs are stably crushed when the hierarchical factor N is increased from 4 to 8, and the folding occurs step by step. However, when the hierarchical factor N is 10 or 12, the central region of the SHTH begins to show a large indentation deformation, especially when the hierarchical factor $N = 12$, as shown in Fig. 16, which is not conducive to EA for the SHTH. This is also the reason why the slopes of SEA and CLE of the SHTHs in Fig. 15 first increase and then decrease.

5.3. Influence of layout of the SHTH

The layout of the honeycomb determines the distribution of the material. Therefore, this section further investigates the out-of-plane mechanical performance of the SHTHs with different layouts of 2×2, 3×4, and 5×6 (reported in Table 8). All honeycombs are within the same cross-sectional area (65 mm $\times$ 60 mm) and have the same mass, 34.91 g.

It is observed from the partial enlargement of Table 8 that all the subtriangles of the SHTH undergo intense plastic strain under
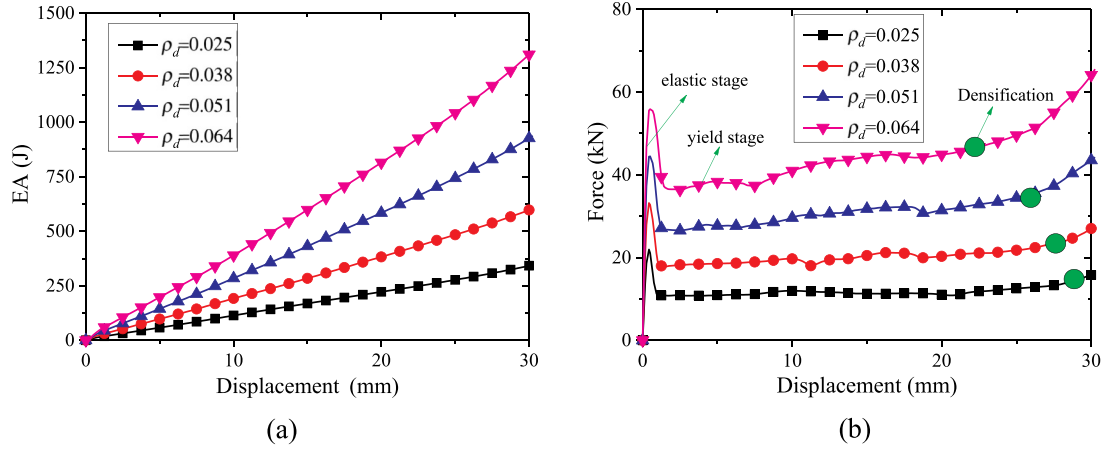
Fig 14. Crashworthiness results of SHTHs under different relative densities: (a) total energy absorption, EA; (b) force-displacement curves.

Table 6
The values of the crashworthiness indicators of SHTHs.

ρ_d	EA (J)	SEA (kJ/kg)	MCF (kN)	CLE (%)
0.025	341.89	9.79	11.39	54.01
0.038	597.26	11.41	19.91	60.78
0.051	926.56	13.31	30.89	69.48
0.064	1310.25	15.01	43.68	78.18

compressive load, and with the increase in honeycomb layouts, the subtriangles have obvious interactive extrusion phenomena (see the red box above). Furthermore, the SEA and collision force curves of the different SHTH layouts are presented in **Fig. 17**. Observably, increasing the number of honeycomb layouts, the SEA and collision force level of the honeycomb have been improved. Moreover, the densification stage of the honeycomb gradually shifts to an earlier displacement, as demonstrated in **Fig. 17**(b).

The crashworthiness indicators of the SHTHs with different layouts are listed in **Table 9**, and a histogram is also given in **Fig. 18**. The SEA, MCF and CLE are significantly enhanced with increasing layout number. When the number of layouts increased from 2 × 2 to 5 × 6, the SEA, MCF and CLE increase by 29.35%, 29.33%, and 37.83%, respectively. On the other hand, the PCF of the SHTH decreases by 7%, which is an advantage that promotes crashworthiness. Conclusively, reasonably increasing the cell layout is an effective method for improving the crashworthiness of the SHTH.

6. Theoretical model of the SHTH

A theoretical model can effectively analyze the mechanical properties of a specific structure at any stage of research and has the advantages of short time consumption and high practicability (Qiu et al., 2015; Yang et al., 2018a; Zhang et al., 2018a). Therefore, theoretical models of a SHTH subjected to an out-of-plane load are developed based on simplified super folding element (SSFE) theory (Chen and Wierzbicki, 2001; Wierzbicki and Abramowicz, 1983) in this section.

A basic element consisting of three extensional triangular elements and three stationary hinge lines shown in **Fig. 19**(a) is proposed based on SSFE theory. The energy consumed by a fully folded wave mainly includes the bending energy Q_b^{total} and the membrane energy Q_m^{total}, and its mathematical expression is as follows:

$$MCF \cdot 2H \cdot \eta = Q_b^{total} + Q_m^{total} \tag{11}$$

where MCF represents the mean crushing force, *2H* represents the length of collision folding wave, and η denotes the collision efficiency coefficient; η is taken as 0.7 in the paper according to (Chen and Wierzbicki, 2001).

6.1. The bending energy

The ideal state of the four rotation angles γ generated at the bending hinge in a folded wave is $\pi/2$ (Xie et al., 2017; Zhang et al., 2018a), as shown in **Fig. 19**(b). Thus, the energy generated by the bending of a fold for a basic element Q_b can be expressed as:

$$Q_b = \sum_{i=1}^{4} M_0 \gamma_i b = 2\pi M_0 b \tag{12}$$

where b is the length of the flange; M_0 is the fully plastic bending moment of the flange, and

$$M_0 = \frac{1}{4}\sigma_0 t^2 \tag{13}$$

where t is the wall thickness of the honeycomb and σ_0 is the flow stress of the material, which can be calculated using the following formula (Tabacu, 2015; Zhang et al., 2018a):

$$\sigma_0 = \sqrt{\frac{\sigma_y \sigma_u}{(1+n)}} \tag{14}$$

where σ_y and σ_u represent the yield stress and ultimate stress of the material, respectively; and n represents the strain hardening index.

Assuming that the bending fold wavelengths of the entire structure are equal, the total bending energy dissipation of the honeycomb Q_b^{total} is expressed as:

$$Q_b^{total} = 2\pi M_0 B \tag{15}$$

where B denotes the total length of all flanges.

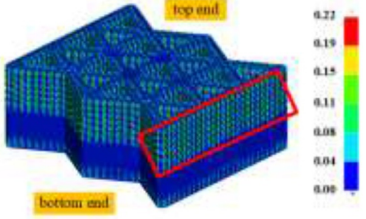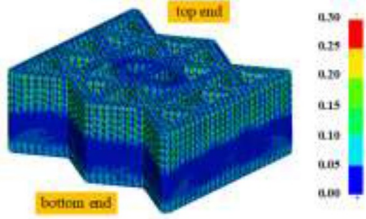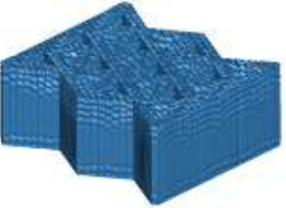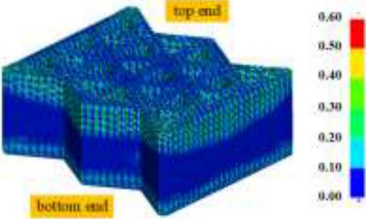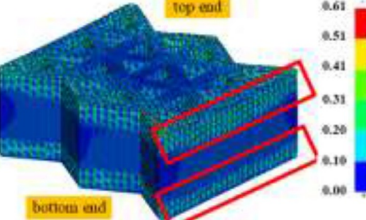### 6.2. The energy dissipated via membrane deformation

To analyze the membrane energy dissipation of the SHTH, the geometrical cross-section of the SHTH is divided into four different corner elements (as shown in **Fig. 20**): a 3-plane element, 4-plane element, 5-plane element and 6-plane element.

The energy membrane dissipation of the 3-plane element, 4-plane element, and 6-plane element can be expressed separately as follows in a folded wavelength (Tran et al., 2014; Xie et al., 2017),

$$Q_m^{3-plane\ element} = 4M_0 \frac{H^2}{t}(1 + 2tan(\theta/2)) = 4M_0 \frac{H^2}{t}(1 + 2tan(30°))$$

$$= 8.619 M_0 \frac{H^2}{t} \tag{16}$$

$$Q_m^{4-plane\ element} = 8M_0 \frac{H^2}{t}(1 + \frac{1}{\cos\beta}) = 8M_0 \frac{H^2}{t}(1 + \frac{1}{\cos 60°}) = 24M_0 \frac{H^2}{t} \tag{17}$$

Table 7
Plastic deformation shapes and strain regions of SHTHs.

ρ_d	Deformation shape	Plastic strain region
0.025		
0.038		
0.051		
0.064		

$$Q_m^{6-plane\ element} = 2Q_m^{II} = 16M_0 \frac{H^2}{t}(1 + \frac{1}{\cos 60°}) = 48M_0\frac{H^2}{t} \tag{18}$$

A 5-plane element is approximated as a combination of a 4-plane element and a special form of a 3-plane element (120°), referring to **Fig. 21**.Then, the membrane dissipation energy of the 5-plane element $Q_m^{5-plane\ element}$ is as follows (Zhang and Zhang, 2012):

$$Q_m^{5-plane\ element} = Q_m^{4-plane\ element} + Q_m^{3-panel\ element\,(120°)}$$

$$= 24M_0\frac{H^2}{t} + 10.041M_0\frac{H^2}{t} = 25.041M_0\frac{H^2}{t} \tag{19}$$

Therefore, the whole energy dissipated by membrane deformation Q_m^{total} of the SHTH is:

$$Q_m^{total} = A_3 Q_m^{3-plane\ element} + A_4 Q_m^{4-plane\ element} + A_5 Q_m^{5-plane\ element}$$

$$+ A_6 Q_m^{6-plane\ element}$$

$$=(8.619A_3 + 24A_4 + 25.041A_5 + 48A_6)M_0\frac{H^2}{t} \tag{20}$$

where A_3, A_4, A_5, and A_6 indicate the number of the 3-plane element, 4-plane element, 5-plane element and 6-plane element for the SHTH, respectively.

6.3. The folding length and mean crushing force

Substituting Eq. (15) and Eq. (20) into Eq. (11):

$$2MCF·H·\eta = 2\pi M_0 B + (8.619A_3 + 24A_4 + 25.041A_5 + 48A_6)M_0\frac{H^2}{t} \tag{21}$$

According to the stationary conditions, the half-wavelength H can be determined as:

$$\frac{\partial MCF}{\partial H} = 0 \tag{22}$$

Therefore,

$$H = \sqrt{\frac{\pi·B·t}{(4.3095A_3 + 12A_4 + 12.5205A_5 + 24A_6)}} \tag{23}$$

Substituting Eq. (23) into Eq. (21) gives the MCF for the SHTH as:

$$MCF = \frac{\sigma_0·k}{2\eta}·\sqrt{(4.3095A_3 + 12A_4 + 12.5205A_5 + 24A_6)·\pi·B}·t^{1.5} \tag{24}$$

where k is the dynamic enhancement factor, which is introduced mainly for considering the inertia effect. k is recommended to be in the range of 1.1–1.6 for an aluminum alloy (HANSSEN et al., 1999; Qiu et al., 2016). k is set to 1.2 in the paper.

Here, the SHTH arranged in a 1 × 2 layout is taken as an example, as shown in **Fig. 20**. Therefore, when $N = 2$, the total section circumference B_2 is 990 mm for the SHTH, and the values of A_3, A_4, A_5, and A_6 are 8, 8, 2, and 11, respectively.

Substituting the data into Eqs. (23) and (24),

(a)

(b)

(c)

(d)
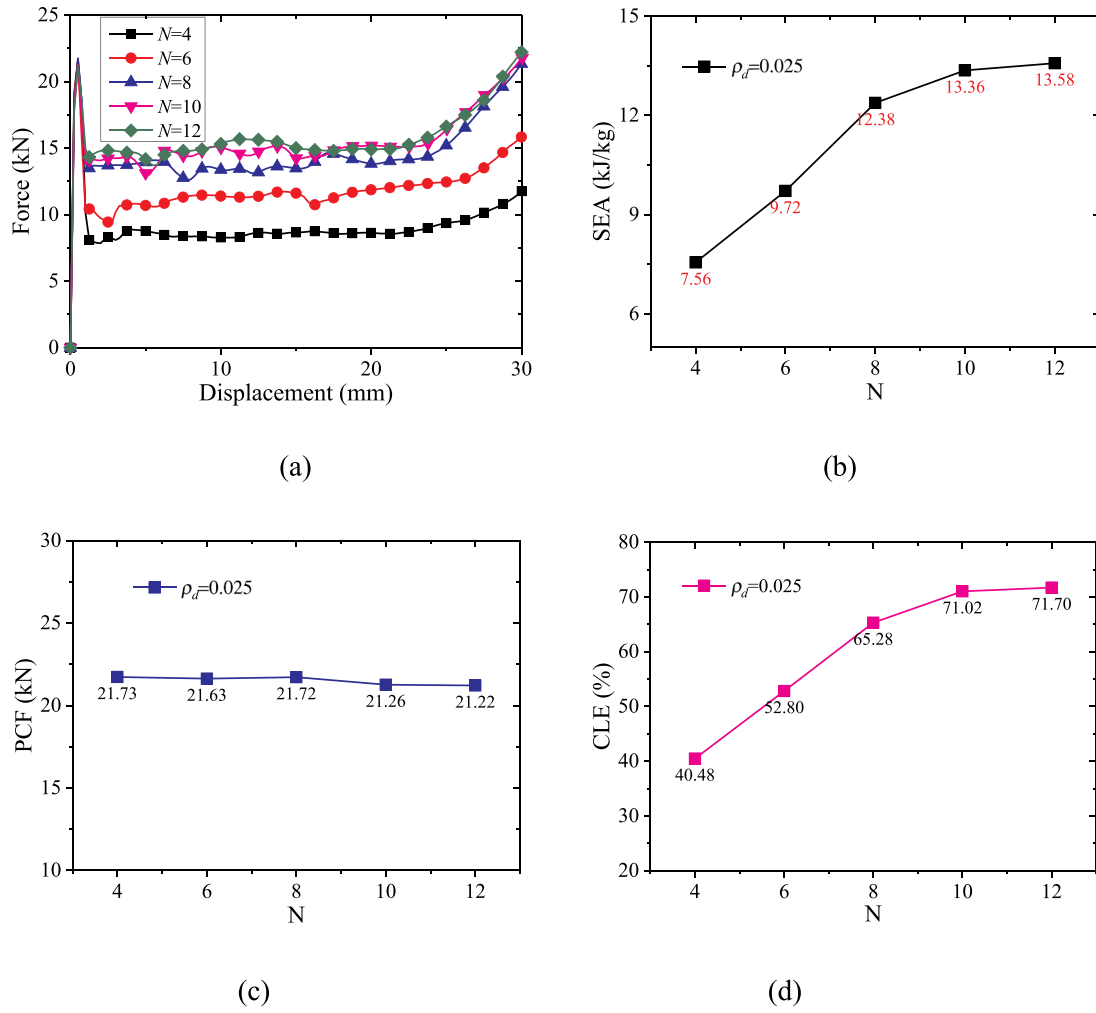
Fig 15. The numerical results of SHTHs with different hierarchical factor *N*: (a) force-displacement curves.

$$H_{N-2} = \sqrt{7.414t} \text{ (mm)} \qquad (25)$$

$$MCF_{N-2} = k\frac{60583.51}{\eta \times 1000}t^{1.5} = \frac{1.2 \times 60583.51}{0.7 \times 1000}t^{1.5} = 103.857\, t^{1.5} \text{ (kN)} \qquad (26)$$

When $N = 3$, the total section circumference B_3 is 1020 mm for the SHTH, and the values of A_3, A_4, A_5, and A_6 are 8, 14, 2, and 19, respectively.
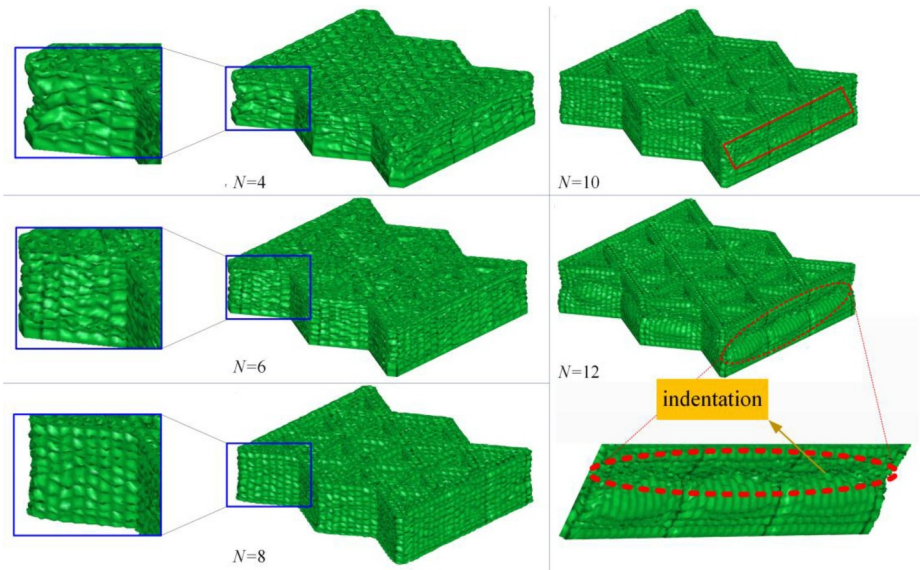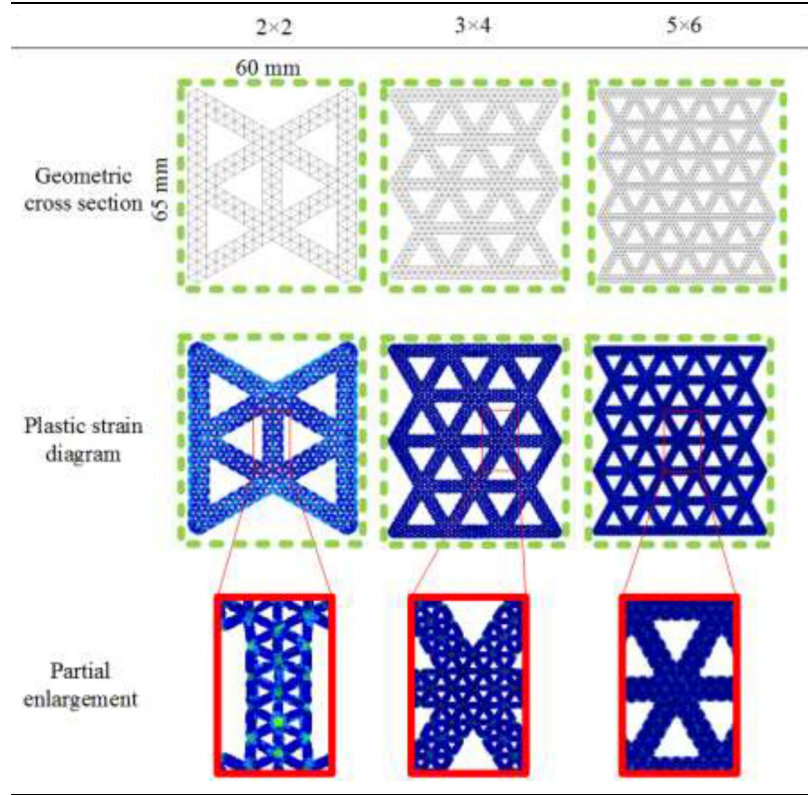

Fig 16. The deformation shapes of SHTHs with different hierarchical factors *N*.

Table 8
Honeycombs with different layouts.

Substituting the data into Eqs. (23) and (24),

$$H_{N-3} = \sqrt{4.688t} \ (\text{mm}) \tag{27}$$

$$MCF_{N-3} = k\frac{78494.065}{\eta \times 1000}t^{1.5} = \frac{1.2 \times 78494.065}{0.7 \times 1000}t^{1.5} = 134.561 \ t^{1.5} \ (\text{kN}) \tag{28}$$

When $N \geq 4$, the total section circumference B_N is $1260 - \frac{720}{N}$ mm for the SHTH, and the values of A_3, A_4, A_5, and A_6 are as follows:

$$\begin{cases} A_3 = 8 \\ A_4 = 12N - 28 \\ A_5 = 2 \\ A_6 = 6N + 5 \end{cases} \tag{29}$$

Table 9
Crashworthiness indicators of the SHTHs with different layouts.

Layouts	EA (J)	SEA (kJ/kg)	MCF (kN)	PCF (kN)	CLE (%)
2 × 2	306.86	8.79	10.23	21.72	47.10
3 × 4	341.88	9.79	11.40	21.09	54.04
5 × 6	396.92	11.37	13.23	20.38	64.92

Therefore, substituting the data into Eqs. (23) and (24),

$$H_{N \geq 4} = \sqrt{\frac{1260 \ N - 720}{91.673 \ N^2 - 49.81 \ N} \cdot t} \ (\text{mm}) \tag{30}$$
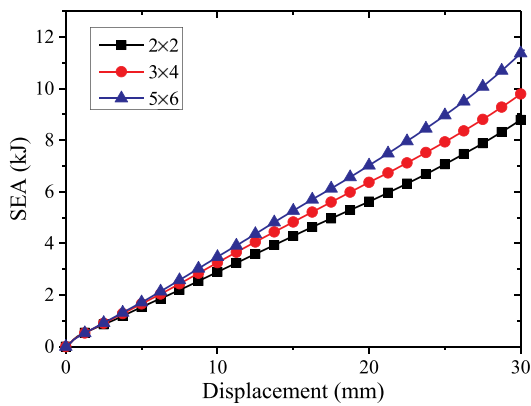
(a)
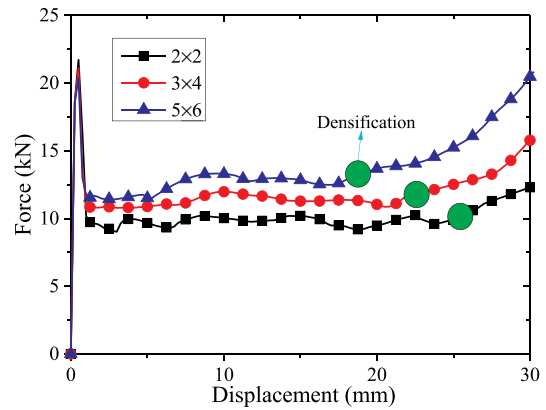
(b)

Fig 17. Crushing responses of SHTHs with different layouts: (a) specific energy absorption, SEA; (b) force-displacement curves.

Fig 18. Comparison of crashworthiness in different layouts: (a) specific energy absorption, SEA; (b) mean crushing force, MCF; (c) peak crushing force, PCF; (d) crushing load efficiency, CLE.

$$MCF_{N\geq4} = \frac{1.2 \times 106.076}{2 \times 0.7 \times 1000} \cdot \sqrt{\pi \cdot (288N - 156.483) \cdot \left(1260 - \frac{720}{N}\right)} \cdot t^{1.5} \text{ (kN)}$$

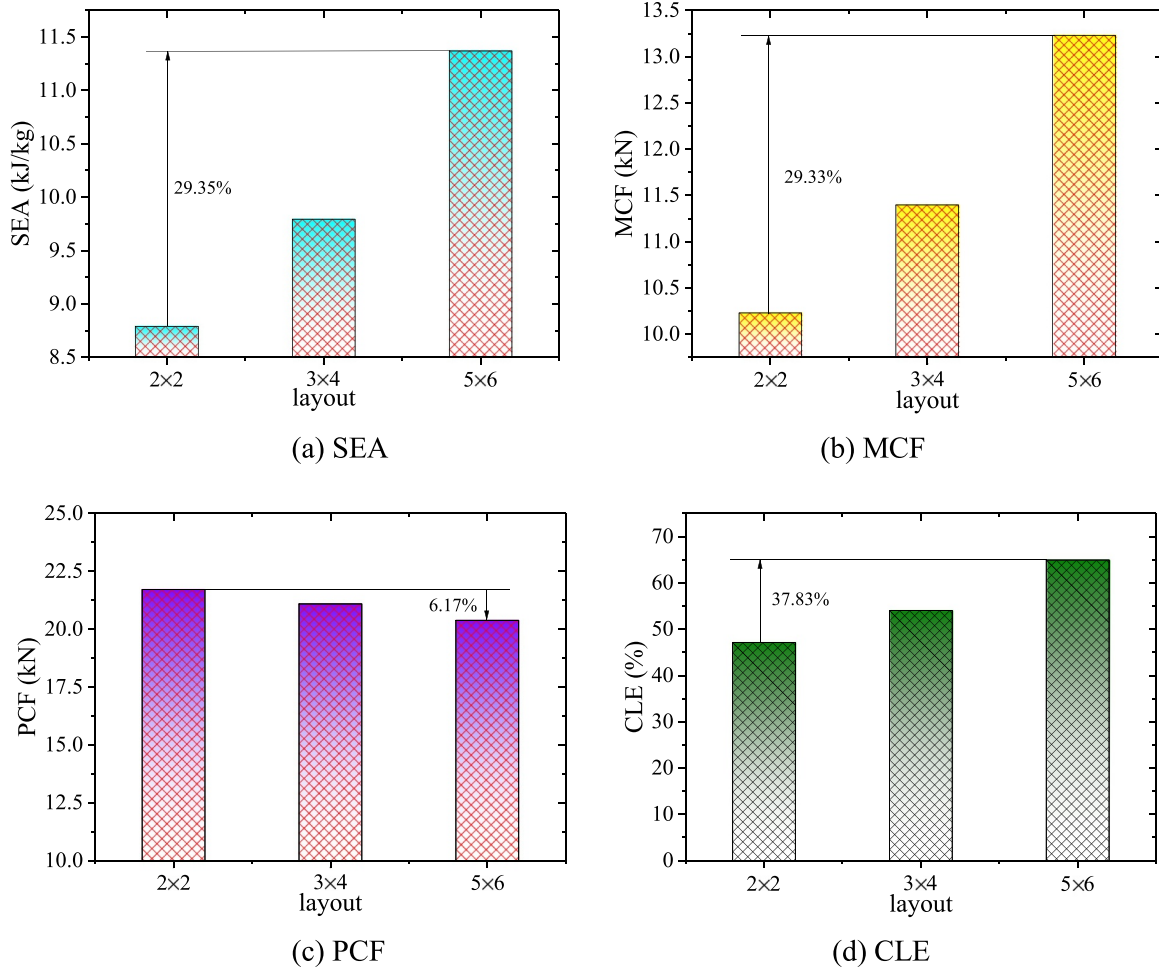$$= \sqrt{(7.480N - 4.064) \cdot \left(1260 - \frac{720}{N}\right)} \cdot t^{1.5}$$

$$(31)$$

6.4. Comparison between theoretical prediction and numerical analysis

Numerical analysis is performed in this section to compare and verify the reliability of the theoretical models derived in Section 6.3. Table 10 gives the detailed numerical values and errors between FE analysis and theoretical prediction for 12 SHTHs with a 1 × 2 layout. It is obvious that the maximal error is 10.05%, which is within an acceptable range. The results demonstrate that the theoretical model established in Section 6.3 is reliable for predicting a SHTH's out-of-plane compression mechanical response.
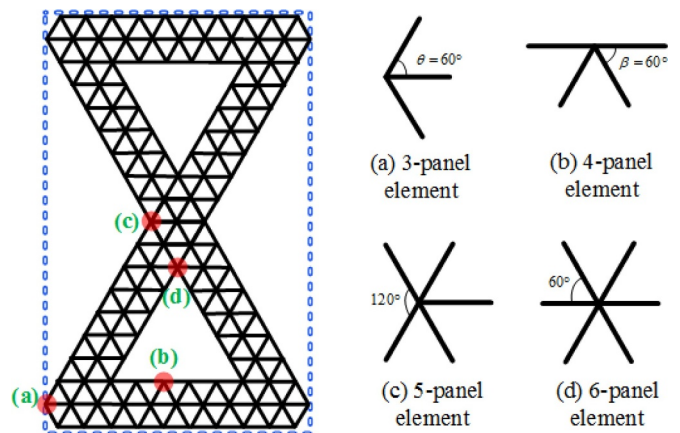

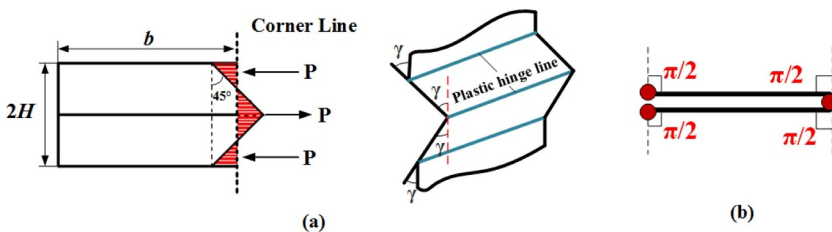**Fig 20.** Classification of the corner elements of honeycomb cross-sections.

Fig 19. Schematic of the flange deformation: (a) bending deformation, (b) complete flattening state.
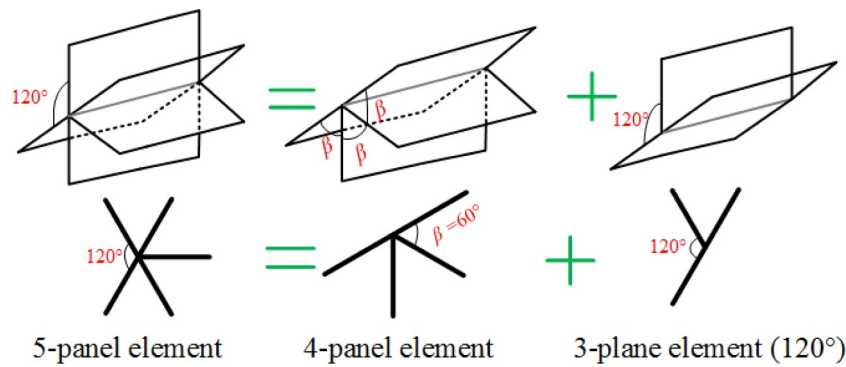
Fig 21. The combination figure of a 5-plane element.

Table 10
Comparison of the SHTH between theoretical prediction (Theo.) and numerical analysis (FEA).

No.	N	t (mm)	MCF (kN) FEA	Error (%) Theo.	
1	2	0.06	1.53	1.39	10.05
2	3	0.04	1.08	1.02	5.88
3	4	0.04	1.34	1.36	−1.70
4	4	0.05	1.87	1.86	0.48
5	4	0.06	2.46	2.33	5.38
6	5	0.04	1.54	1.60	−3.38
7	5	0.05	2.16	2.12	1.54
8	5	0.06	2.83	2.74	3.32
9	6	0.06	3.17	3.33	−4.89
10	6	0.07	3.99	4.11	−2.88
11					
	8	0.06	3.75	4.10	−8.43
12	8	0.07	4.73	5.03	−6.00

7. Conclusions

This paper investigated the out-of-plane crushing mechanical behaviors of a novel SHTH via experiments, simulations and theoretical analysis. The deformation shapes, loading capacities and energy absorption of the SHTH were investigated in detail. Several conclusions can be drawn as follows:

1) The side hierarchical design is an effective means for improving the crashworthiness of honeycomb structures. The SHTH has a higher collision force level and better EA than the OTH and DTH. The SEA of the SHTH is 79.3% and 175.9% greater than those of the OTH and DTH, respectively, with the same mass.

2) An increase in the relative density can change the deformation shape of a SHTH from collapse at one end to collapse at both ends, which makes the SEA and CLE of the SHTH increase by 53% and 45%, respectively.

3) The EA and load bearing efficiency of the SHTH approach the maximum and become stable when the hierarchical factor N is close to 10. Furthermore, increasing the number of honeycomb layouts can improve the SEA and collision force level of honeycombs, but the densification stage of the honeycomb gradually shifts to an earlier displacement.

4) A theoretical model with good prediction accuracy is developed and validated for the SHTH based on the SSFE and numerical simulation.

Declaration of Competing Interest

None.

Appendix

Table A1.

Table A1
All the acronyms with their full name or explanation in this paper.

Acronym	Full name or explanation
SHTH	side hierarchical triangular honeycomb
OTH	ordinary triangular honeycomb
DTH	double-triangular honeycomb
SSFE	simplified super folding element theory
SLS	selective laser sintering technology
WEDM	wire-cut electrical discharge machining
$SHTH_2$	side hierarchical triangular honeycomb ($N = 2$) with a layout of 2×2
$PC\text{-}SHTH_5$	primary triangle substructure ($N = 5$) with a layout of 2×2
UMTM	universal material testing machine
LSTC	Livermore Software Technology Corporation
SEA	specific energy absorption
EA	total energy absorption
PCF	peak crushing force
MCF	mean crushing force
CLE	crushing load efficiency
N	hierarchical factor

References

Abo Sabah, S.H., Kueh, A.B.H., Al-Fasih, M.Y., 2017. Comparative low-velocity impact behavior of bio-inspired and conventional sandwich composite beams. Compos. Sci. Technol. 149, 64–74.

Ajdari, A., Jahromi, B.H., Papadopoulos, J., Nayeb-Hashemi, H., Vaziri, A., 2012. Hierarchical honeycombs with tailorable properties. Int. J. Solids Struct. 49, 1413–1419.

An, B., Zhao, X., Zhang, D., 2014. On the mechanical behavior of bio-inspired materials with non-self-similar hierarchy. J. Mech. Behav. Biomed. Mater. 34, 8–17.

Ashab, A., Dong, R., Lu, G., Xu, S., Wen, C., 2015. Experimental investigation of the mechanical behavior of aluminum honeycombs under quasi-static and dynamic indentation. Mater. Des. 74, 138–149.

Balawi, S., Abot, J.L., 2008. The effect of honeycomb relative density on its effective in-plane elastic moduli: an experimental study. Compos. Struct. 84, 293–299.

Baroutaji, A., Sajjia, M., Olabi, A.-G., 2017. On the crashworthiness performance of thin-walled energy absorbers: recent advances and future developments. Thin-Walled Struct. 118, 137–163.

Belouettar, S., Abbadi, A., Azari, Z., Belouettar, R., Freres, P., 2009. Experimental investigation of static and fatigue behaviour of composites honeycomb materials using four point bending tests. Compos. Struct. 87, 265–273.

Chen, T., Zhang, Y., Lin, J., Lu, Y., 2019. Theoretical analysis and crashworthiness optimization of hybrid multi-cell structures. Thin-Walled Struct. 142, 116–131.

Chen, W., Wierzbicki, T., 2001. Relative merits of single-cell, multi-cell and foam-filled thin-walled structures in energy absorption. Thin-Walled Struct. 39, 287–306.

Chen, Y., Wang, J., Sun, J., Mao, C., Wang, W., Pan, H., Tang, R., Gu, X., 2014. Hierarchical structure and mechanical properties of remineralized dentin. J. Mech. Behav. Biomed. Mater. 40, 297–306.

Crupi, V., Epasto, G., Guglielmino, E., 2013. Comparison of aluminium sandwiches for lightweight ship structures: honeycomb vs. foam. Mar. Struct. 30, 74–96.

Fan, H., Luo, Y., Fan, Y., Li, W., 2018. Approaching perfect energy absorption through structural hierarchy. Int. J. Eng. Sci. 130, 12–32.

Fang, J., Gao, Y., Sun, G., Qiu, N., Li, Q., 2015a. On design of multi-cell tubes under axial and oblique impact loads. Thin-Walled Struct. 95, 115–126.

Fang, J., Gao, Y., Sun, G., Zheng, G., Li, Q., 2015b. Dynamic crashing behavior of new extrudable multi-cell tubes with a functionally graded thickness. Int. J. Mech. Sci. 103, 63–73.

Fang, J., Sun, G., Qiu, N., Kim, N.H., Li, Q., 2017. On design optimization for structural crashworthiness and its state of the art. Struct. Multidiscip. Optim. 55, 1091–1119.

Fang, J., Sun, G., Qiu, N., Pang, T., Li, S., Li, Q., 2018. On hierarchical honeycombs under out-of-plane crushing. Int. J. Solids Struct. 135, 1–13.

Hallquist, J.O., 2003. LS-DYNA Keyword User's Manual. California: Livemove Software. Technology Corporation.

Hanssen, A., G., H., O., S., 1999. Static and dynamic crushing of square aluminium extrusions with aluminium foam filler. Int. J. Impact Eng. 24, 475–507.

Hao, P., Du, J., 2018. Energy absorption characteristics of bio-inspired honeycomb column thin-walled structure under impact loading. J. Mech. Behav. Biomed. Mater. 79, 301–308.

Hohe, J., Becker, W., 2003. Effective mechanical behavior of hyperelastic honeycombs and two-dimensional model foams at finite strain. Int. J. Mech. Sci. 45, 891–913.

Korsunsky, A., 2014. Thermal-mechanical Behaviour of the Hierarchical Structure of Human Dental Tissue. University of Oxford.

Lee, H.S., Hong, S.H., Lee, J.R., Kim, Y.K., 2002. Mechanical behavior and failure process during compressive and shear deformation of honeycomb composite at elevated temperatures. J. Mater. Sci. 37, 1265–1272.

Liu, J., Wang, Z., Hui, D., 2018. Blast resistance and parametric study of sandwich structure consisting of honeycomb core filled with circular metallic tubes. Compos. Part B 145, 261–269.

Meng, F.X., Zhou, Q., Yang, J.L., 2009. Improvement of crashworthiness behaviour for simplified structural models of aircraft fuselage. Int. J. Crashworthiness 14, 83–97.

Murthy, P.L.N., Chamis, C.C., Singhal, S.N., 1993. Hierarchical Nonlinear Behavior of Hot Composite Structures. Nasa Sti/recon Technical Report N. 94.

Qiu, N., Gao, Y., Fang, J., Feng, Z., Sun, G., Li, Q., 2015. Crashworthiness analysis and design of multi-cell hexagonal columns under multiple loading cases. Finite Elem. Anal. Des. 104, 89–101.

Qiu, N., Gao, Y., Fang, J., Feng, Z., Sun, G., Li, Q., 2016. Theoretical prediction and optimization of multi-cell hexagonal tubes under axial crashing. Thin-Walled Struct. 102, 111–121.

Sezgin, F.E., Tanoglu, M., Eğilmez, O., Donmez, C., 2010. Mechanical behavior of polypropylene-based honeycomb-core composite sandwich structures. J. Reinf. Plast. Compos. 29, 1569–1579.

Sun, F., Lai, C., Fan, H., 2016a. In-plane compression behavior and energy absorption of hierarchical triangular lattice structures. Mater. Des. 100, 280–290.

Sun, G., Jiang, H., Fang, J., Li, G., Li, Q., 2016b. Crashworthiness of vertex based hierarchical honeycombs in out-of-plane impact. Mater. Des. 110, 705–719.

Sun, G., Zhang, J., Li, S., Fang, J., Wang, E., Li, Q., 2019. Dynamic response of sandwich panel with hierarchical honeycomb cores subject to blast loading. Thin-Walled Struct. 142, 499–515.

Sun, Y., Pugno, N.M., 2013. In plane stiffness of multifunctional hierarchical honeycombs with negative Poisson's ratio sub-structures. Compos. Struct. 106, 681–689.

Tabacu, S., 2015. Axial crushing of circular structures with rectangular multi-cell insert. Thin-Walled Struct. 95, 297–309.

Taylor, C.M., Smith, C.W., Miller, W., Evans, K.E., 2011. The effects of hierarchy on the in-plane elastic properties of honeycombs. Int. J. Solids Struct. 48, 1330–1339.

Taylor, C.M., Smith, C.W., Miller, W., Evans, K.E., 2012. Functional grading in hierarchical honeycombs: density specific elastic performance. Compos. Struct. 94, 2296–2305.

Tran, T., Hou, S., Han, X., Tan, W., Nguyen, N., 2014. Theoretical prediction and crashworthiness optimization of multi-cell triangular tubes. Thin-Walled Struct. 82, 183–195.

Wang, J., Zhang, Y., He, N., Wang, C.H., 2018. Crashworthiness behavior of Koch fractal structures. Mater. Des. 144, 229–244.

Wang, Z., Zhou, Y., Wang, X., Zhang, X., 2016. Multi-objective optimization design of a multi-layer honeycomb sandwich structure under blast loading. Proc. Inst. Mech. Eng. Part D 231, 1449–1458.

Wierzbicki, T., Abramowicz, W., 1983. On the crushing mechanics of thin-walled structures. J. Appl. Mech. 50, 727–734.

Wu, S., Zheng, G., Sun, G., Liu, Q., Li, G., Li, Q., 2016. On design of multi-cell thin-wall structures for crashworthiness. Int. J. Impact Eng. 88, 102–117.

Xiang, J., Du, J., 2017. Energy absorption characteristics of bio-inspired honeycomb structure under axial impact loading. Mater. Sci. Eng. 696, 283–289.

Xie, S., Yang, W., Wang, N., Li, H., 2017. Crashworthiness analysis of multi-cell square tubes under axial loads. Int. J. Mech. Sci. 121, 106–118.

Xu, X., Zhang, Y., Chen, X., Liu, Z., Xu, Y., Gao, Y., 2019. Crushing behaviors of hierarchical sandwich-walled columns. Int. J. Mech. Sci. 105021, 161–162.

Yang, X., Ma, J., Sun, Y., Yang, J., 2018a. Ripplecomb: a novel triangular tube reinforced corrugated honeycomb for energy absorption. Compos. Struct. 202, 988–999.

Yang, X., Sun, Y., Yang, J., Pan, Q., 2018b. Out-of-plane crashworthiness analysis of bio-inspired aluminum honeycomb patterned with horseshoe mesostructure. Thin-Walled Struct. 125, 1–11.

Yin, H., Huang, X., Scarpa, F., Wen, G., Chen, Y., Zhang, C., 2018. In-plane crashworthiness of bio-inspired hierarchical honeycombs. Compos. Struct. 192, 516–527.

Zhang, L., Bai, Z., Bai, F., 2018a. Crashworthiness design for bio-inspired multi-cell tubes with quadrilateral, hexagonal and octagonal sections. Thin-Walled Struct. 122, 42–51.

Zhang, P., Arceneaux, D.J., Khattab, A., 2018b. Mechanical properties of 3D printed polycaprolactone honeycomb structure. J. Appl. Polym. Sci. 135 (12), 46018.

Zhang, X., Zhang, H., 2012. Numerical and theoretical studies on energy absorption of three-panel angle elements. Int. J. Impact Eng. 46, 23–40.

Zhang, Y., Liu, T., Ren, H., Maskery, I., Ashcroft, I., 2018c. Dynamic compressive response of additively manufactured AlSi10Mg alloy hierarchical honeycomb structures. Compos. Struct. 195, 45–59.

Zhang, Y., Lu, M., Wang, C.H., Sun, G., Li, G., 2016. Out-of-plane crashworthiness of bio-inspired self-similar regular hierarchical honeycombs. Compos. Struct. 144, 1–13.

Zhang, Y., Sun, G., Xu, X., Li, G., Li, Q., 2014. Multiobjective crashworthiness optimization of hollow and conical tubes for multiple load cases. Thin-Walled Struct. 82, 331–342.

Zhang, Y., Wang, J., Wang, C., Zeng, Y., Chen, T., 2018d. Crashworthiness of bionic fractal hierarchical structures. Mater. Des. 158, 147–159.

Zhang, Y., Xu, X., Wang, J., Chen, T., Wang, C.H., 2018e. Crushing analysis for novel bio-inspired hierarchical circular structures subjected to axial load. Int. J. Mech. Sci. 140, 407–431.

Zhi, S., 2016. On compressive properties of composite sandwich structures with grid reinforced honeycomb core. Compos. Part B 94, 245–252.

Zhu, H.X., 2010. Effects of relative density and material distribution on the elastic properties and yield strength of metallic honeycombs. Mater. Sci. Forum 638–642, 1003–1008.